University of Groningen

# Semiconducting Polymer Composite Based Bipolar Transistors

Piliego, Claudia; Szendrei, Krisztina; Loi, Maria Antonietta

*Published in:*
Semiconducting Polymer Composites: Principles, Morphologies, Properties and Applications

**IMPORTANT NOTE: You are advised to consult the publisher's version (publisher's PDF) if you wish to cite from it. Please check the document version below.**

*Document Version*
Publisher's PDF, also known as Version of record

*Publication date:*
2013

Link to publication in University of Groningen/UMCG research database

*Citation for published version (APA):*
Piliego, C., Szendrei, K., & Loi, M. A. (2013). Semiconducting Polymer Composite Based Bipolar Transistors. In X. Yang (Ed.), *Semiconducting Polymer Composites: Principles, Morphologies, Properties and Applications* (pp. 457-487). s.n..

**Copyright**
Other than for strictly personal use, it is not permitted to download or to forward/distribute the text or part of it without the consent of the author(s) and/or copyright holder(s), unless the work is under an open content license (like Creative Commons).

The publication may also be distributed here under the terms of Article 25fa of the Dutch Copyright Act, indicated by the "Taverne" license. More information can be found on the University of Groningen website: https://www.rug.nl/library/open-access/self-archiving-pure/taverne-amendment.

**Take-down policy**
If you believe that this document breaches copyright please contact us providing details, and we will remove access to the work immediately and investigate your claim.

*Downloaded from the University of Groningen/UMCG research database (Pure): http://www.rug.nl/research/portal. For technical reasons the number of authors shown on this cover page is limited to 10 maximum.*

Download date: 03-06-2022

# 16
# Semiconducting Polymer Composite Based Bipolar Transistors

*Claudia Piliego, Krisztina Szendrei, and Maria Antonietta Loi*

## 16.1
## Introduction

Since the realization of the first field-effect transistor (FET) in 1928 [1], the electronic devices have been optimized to the point that they have become essential building blocks of today's electronics. The efficient electronic circuit design and their mass production are based on the integration of tiny FETs in single chips with improved performance and reliability. The manufacturing of electronic devices has been dominated by the silicon technology; however, in the past 10 years [2], a new class of semiconductors, based on organic compounds, has also entered into the world of FETs. Plastic transistors, fabricated using organic materials for the active layer, could serve as key components in cheap and flexible electronic devices [3] such as radio frequency identification (RF-ID) tags [4] and flexible displays [5, 6]. Unlike most of the inorganic semiconductors, organic materials can be processed onto various flexible plastic substrates, thanks to their mechanical properties. Moreover, the simplification of the manufacturing processes, by introducing solution processing, and the vapor deposition at low temperature, opens the way toward large area, low-cost fabrication of electronic devices.

The performance of organic semiconductor field-effect transistor has been improved tremendously in the last few years, focusing on increasing the environmental stability and charge carrier mobility of p- and n-type polymers and small molecules. In particular, for polymers the record mobility values reported till date are approaching $2\,\text{cm}^2\ (\text{V}^{-1}\,\text{s}^{-1})$ for p-type polymers [7] and $1\,\text{cm}^2\ (\text{V}^{-1}\,\text{s}^{-1})$ for n-type polymers [8]. The p-type conduction has been till last few years much superior than n-type one, due to the oxygen and water sensitivity of many organic anions [9]. Only recently, n-type polymers with comparable performance have been reported.

Complementary metal oxide–semiconductor (CMOS) technology is the fundamental technology for integrated circuit fabrication. Typically in silicon technology complementary and symmetrical pairs of p- and n-type transistors are used for logic functions. In the case of organic semiconductors several different strategies have been investigated to fabricate a single FET having the functionality of the

*Semiconducting Polymer Composites: Principles, Morphologies, Properties and Applications*, First Edition.
Edited by Xiaoniu Yang.
© 2012 Wiley-VCH Verlag GmbH & Co. KGaA. Published 2012 by Wiley-VCH Verlag GmbH & Co. KGaA.

complementary symmetrical pair of n- and p-type transistors [10]. Bipolar (ambipolar) transistors are able to provide p- and n-channel functionality by using single components [11], bilayers [12], and blends [13–15] as active semiconducting layer. One of the major challenges in achieving good bipolar transport is the efficient injection of holes and electrons from the same metal electrode into the HOMO (highest occupied molecular orbital) and the LUMO (lowest unoccupied molecular orbital) of the semiconductor(s), respectively. Most organic semiconductors have band gaps in the range of 2–3 eV, resulting in a high injection barrier for at least one of the charge carriers, when a single electrode material is employed. The combination of two organic semiconductors in a bilayer or blend, as in the bulk heterojunction configuration, can provide a great opportunity to overcome this limitation. If the materials are warily chosen, the work function of the electrodes could line up properly with the HOMO of one semiconductor for hole injection and with the LUMO of the other for electron injection.

This chapter concentrates on organic bipolar transistors, including details about the basic operation principles, device configurations, and processing methods, and describing the various strategies that have been applied to achieve ambipolar transport. Touching upon small molecule-based FETs and the hybrid approach, the main focus will be on polymer-based bipolar transistors since they can provide one of the ultimate solutions for simple, low-cost fabrication of flexible bipolar FETs.

## 16.2 Basics of Organic Field-Effect Transistors

### 16.2.1 Operation Principles of FETs

A field-effect transistor is basically a three-terminal electrical switch that is able to modulate the flow of current. The three terminals are (Figure 16.1a): the gate electrode, which is separated from the semiconducting layer by a dielectric layer, and the so-called source and drain electrodes, which are in direct contact with the semiconductor layer. The position of these two electrodes defines the geometrical characteristics of the device, that are, the channel width ($W$) and length ($L$). By applying voltage to the gate it is possible to control the current flowing between the source and the drain in the semiconducting active layer. The gate electrode is most commonly a heavily doped silicon wafer, but also a metal or a conducting polymer can serve as the gate electrode. Gate dielectrics can be oxides, such as $SiO_2$ (especially when doped silicon is used as gate) and $Al_2O_3$, or polymeric insulators, such as PMMA (poly(methyl methacrylate)) and many others recently synthetized [16, 17]. The organic semiconducting layer can be applied by vapor deposition (sublimation) or solution processing. The vacuum sublimed small molecule layers generally yield better transistor performance due to higher crystallinity and controllable morphology, although solution processing of small molecules and polymer has the potential for low cost and high volume production. The source and drain electrodes for

charge injection are usually fabricated using high work function metals (Au, Ag, Pd, Pt) or conducting polymers (PEDOT:PSS).

#### 16.2.1.1 Unipolar FETs

Figure 16.1 illustrates the typical operation regimes of a unipolar FET where only one type of charge carriers (holes or electrons) can accumulate in the channel depending on the nature of the semiconductor. In operation conditions, a voltage is applied to the drain ($V_d$) and gate ($V_g$) electrode while the source electrode is grounded ($V_s = 0$). The difference between the potential at source and drain is the source–drain voltage ($V_{ds}$), while the potential difference between the source and the gate is called the gate voltage ($V_g$). The gate itself is isolated from the source and drain by an insulator (dielectric); therefore in ideal conditions no current flows through the dielectric. The charge-injecting electrode is the source, which injects electrons or holes into the channel depending on the polarity with respect to the gate electrode. When a positive voltage is applied to the gate electrode, electrons accumulate at the semiconductor–dielectric interface. The opposite situation occurs for a negatively applied gate voltage; positive charges accumulate at the semiconductor–dielectric interface. When a voltage higher than the threshold voltage ($V_{th}$) is reached, there will be the formation of a conductive channel from the source to the drain, allowing current to flow. The threshold voltage is mostly due to deep traps in the active layer, which reduce the contribution of induced charges to the current flow. These deep traps first have to be filled, making the effective gate voltage $V_g - V_{th}$. At higher gate voltage more charge carriers will accumulate, causing an extension of the conductive channel. In this manner the gate voltage controls the conductivity between the source and the drain. The transistor can operate in two regimes, the linear and the saturation regimes. In the so-called linear

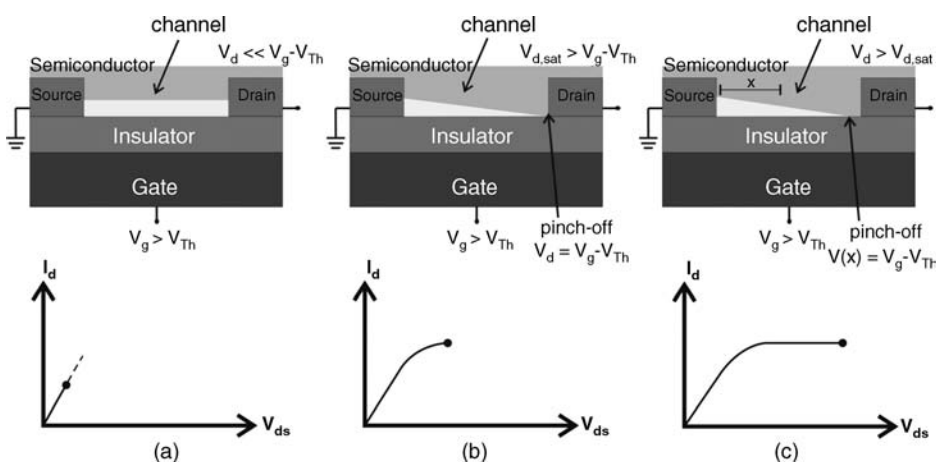


**Figure 16.1** Operating regimes of a unipolar FET: schematic of a typical FET and graph representation of the linear regime (a), the pinch off point (b), and the saturation regime (c). (Reprinted with permission from Ref. [18]).

regime, when a small source–drain bias is applied ≪ ($V_{sd} \ll V_g$) (Figure 16.1a) and $V_g > V_{th}$, current starts flowing in the channel and it is directly proportional to the $V_{ds}$. When $V_{ds}$ is further increased and reaches the pinch off point ($V_{ds} = V_g - V_{th}$), a depletion region forms next to the drain electrode, since the difference between the gate voltage and the local potential ($V_x$) is below the $V_{th}$ (Figure 16.1b). This narrow depletion region allows the flow of a space-charge limited saturation current ($I_{ds,sat}$) from the pinch off point to the drain. Further increasing $V_{ds}$ (Figure 16.1c) expands the depletion region, shortens the channel, and the current saturates at $I_{ds,sat}$ since the potential drop between the pinch off point and the source electrode stays approximately constant.

#### 16.2.1.2 Bipolar FETs

The current in FETs with bipolar nature is composed of both electrons and holes, with proportion depending on the bias conditions. The typical operating regimes for a bipolar FET are illustrated in Figure 16.2 [19]. In regime 1 when $|V_g – V_{th}| > |V_{ds}|$ and they are both positive, the current is dominated by electrons, similarly to the unipolar electron transport. While in regime 4 when $|V_g – V_{th}| > |V_{ds}|$, but both voltages are negative, the current is carried by holes and the bipolar FET operates as unipolar p-type FET. In regime 6, when $V_g – V_{th}$ is positive and $V_{ds}$ is negative, the

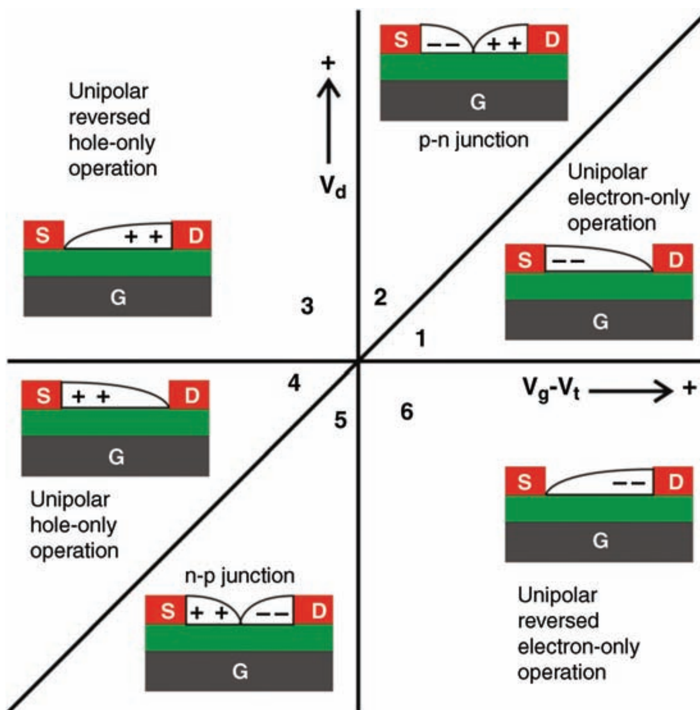


**Figure 16.2** Illustration of all operating regimes for a bipolar FET. (Reprinted with permission from Ref. [20]).

effective gate potential becomes positive throughout the whole channel and the bipolar FET behaves as it was a unipolar n-type FET where the source and drain electrodes are inverted. Likewise, when $V_g$–$V_{th}$ is negative and $V_{ds}$ is positive, the effective gate potential is negative in the channel and the bipolar FET operates as a unipolar p-type FET where the source and drain electrodes are inverted.

Bipolarity only occurs in regimes 2 and 5 where $V_{ds} > V_g - V_{th} > 0$ and $V_{ds} < V_g - V_{th} < 0$, respectively. Under these bias conditions a unipolar transistor operates in the saturation regime and charges cannot be accumulated in the pinched off part of the channel. However, under these conditions, the effective gate potential changes sign at a certain position in the channel in a bipolar FET. As a result, holes and electrons accumulate at the opposite sides of the FET and are separated by a narrow transition region acting as a p–n junction.

## 16.2.2 Current–Voltage Characteristics

### 16.2.2.1 Unipolar FET

The current–voltage characteristics of a unipolar p-type FET in linear and saturation regime are illustrated in Figure 16.3 [16]. Figure 16.3a shows the typical output characteristics, where the drain current is plotted against the source–drain voltage at different constant gate voltages. The linear and saturation regimes are obtained at low and high $V_{ds}$, respectively. Figure 16.3b illustrates the drain current versus the gate voltage (transfer characteristic) in the linear regime ($V_{ds} \ll V_g$) both on a semilogarithmic and a linear scale. The semilogarithmic plot provides the so-called onset voltage ($V_{on}$) where the drain current starts to increase sharply. From the linear plot the linear field-effect mobility can be extracted since the gradient of the current increase is directly

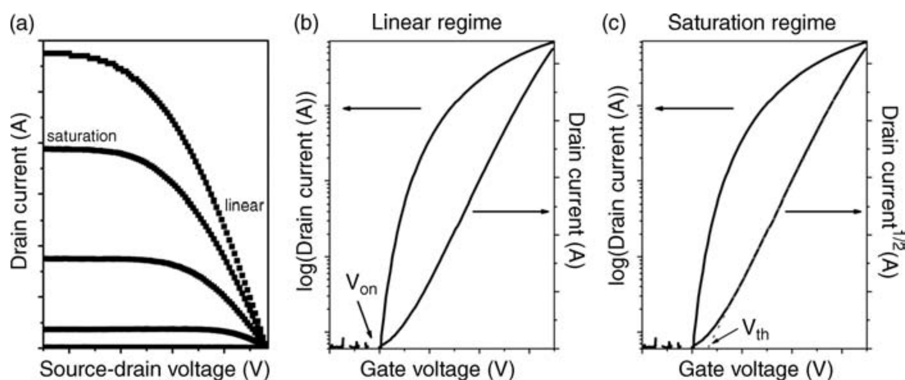


**Figure 16.3** Typical current–voltage characteristics of a unipolar n-type FET: (a) output characteristics showing the linear and saturation regimes; (b) transfer characteristics in the linear regime indicating the onset voltage ($V_{on}$); (c) transfer characteristics in the saturation regime indicating the threshold voltage ($V_{th}$).

proportional to the mobility according to the following equation:

$$\mu_{\text{lin}} = \frac{\partial I_{\text{ds}}}{\partial V_{\text{g}}} \times \frac{L}{WCV_{\text{ds}}}. \tag{16.1}$$

Figure c represents the transfer characteristics in the saturation regime. In this plot the extrapolation of the linear fit gives the threshold voltage ($V_{\text{th}}$) while the square root of the drain current can be used to calculate the saturation mobility depending on the gate voltage according to Eq. (16.2):

$$\mu_{\text{sat}} = \left(\frac{\partial\sqrt{I_{\text{ds,sat}}}}{\partial V_{\text{g}}}\right)^2 \times \frac{2L}{WC}. \tag{16.2}$$

Another important feature of the transfer curves is the $I_{\text{on}}/I_{\text{off}}$ ratio that is defined as the ratio of the drain current in the on-state at a given gate voltage and the drain current in the off state. To obtain excellent switching properties, this ratio has to be maximized.

#### 16.2.2.2 **Bipolar FETs**

The transfer and output curves of a bipolar FET are more complex [16]. The output curve, illustrated in Figure 16.4a, shows the superposition of the standard saturation behavior for one of the charge carriers at higher $V_{\text{g}}$ and a superlinear current increase at lower $V_{\text{g}}$ and high $V_{\text{ds}}$ due to the injection of the opposite charge carriers. The transfer curve (Figure 16.4b) has a unique V-shape where the left arm represents the hole transport and the right arm corresponds to the electron transport.

### 16.2.3 Device Configurations

The different transistor geometries can strongly influence the device performance. The most commonly used configurations are top contact/bottom gate (TC/BG),

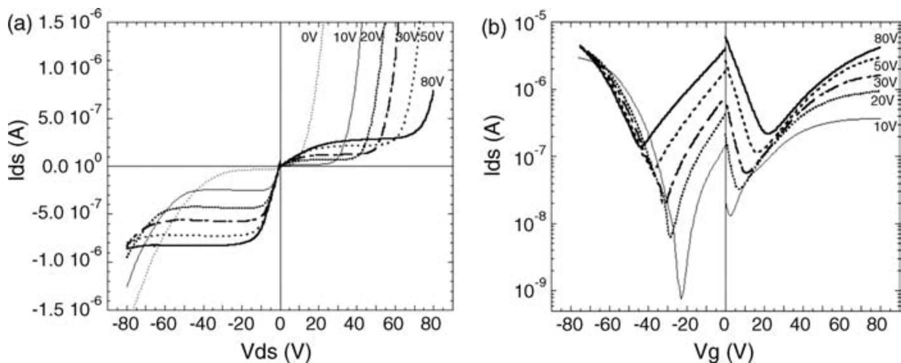


**Figure 16.4** (a) Transfer and (b) output characteristics of a bipolar FET. (Reprinted with permission from Ref. [21]).

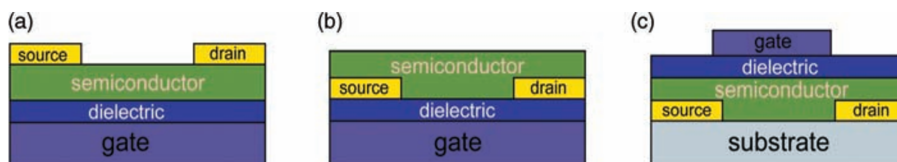


**Figure 16.5** Typical FET configurations: (a) top contact/bottom gate (TC/BG), (b) bottom contact/bottom gate (BC/BG) and (c) bottom contact/top gate (BC/TG).

bottom contact/bottom gate (BC/BG), and bottom contact/top gate (BC/TG) (Figure 16.5). The main difference among these configurations is the position of the charge injecting electrodes with respect to the gate electrode. In the BC/BG geometry, the charges can be directly injected into the channel at the interface of the semiconductor and the dielectric while in the two other geometries, TC/BG and BC/TG, the electrodes are separated from the channel by the semiconductor. In the last two structures the current is larger since charges can be injected not only from the edges of the electrodes but also from the overlapping area with the gate electrode [22]. The properties of the interface between the electrodes and the semiconductor and between the dielectric and the semiconductor are very critical and can greatly affect the device performance.

### 16.2.4
### Role of the Injecting Electrodes

In order to obtain reasonable FET performance, the injection of electrons and holes from the source electrode into the semiconductor has to be ensured. Good ohmic contact between the metal electrode and the semiconductor can be achieved when the work function of the metal is closely aligned with the LUMO or the HOMO of the material for the injection of electrons or holes, respectively [23]. Without proper alignment, a potential barrier will form, depending on the difference between the work function of the electrode and the energy levels of the semiconductor. This will lead to poor injection and increased resistance of the transistor. Non ohmic contacts result in irregularities in the linear regime of the output characteristics of the transistor (i.e., primary suppression and superlinear current increase). High-contact resistance has similar effect due to a source–drain voltage drop at the contacts. The potential barrier can be reduced by choosing the appropriate injecting electrode or introducing dipoles at the metal surface with self-assembled monolayers that are able to modify (increase or decrease) the metal work function [24].

The position of the injecting electrode also affects the contact resistance. Contrary to BC/BG, in BC/TG and TC/BG configurations, where the source and drain electrodes overlap with the gate electrode, the contact resistance is lower since the charges are injected from a larger area. Moreover, evaporated top metals can introduce surface states in the semiconductor facilitating or hindering the charge injection [25].

In the fabrication of bipolar transistors, one of the major challenges is the efficient injection of both carriers into the HOMO and LUMO of the semiconductor(s). This can be achieved by using one single electrode in combination with two semiconductor materials or two injecting electrodes with different work functions.

### 16.2.5 Applications: Inverters and Light-Emitting Transistors

The development of low cost, good performing bipolar FETs is highly desirable for CMOS inverter technology and light-emitting field-effect transistors (LE-FETs). Several groups have already demonstrated discrete inverters [13, 26, 27] and simple circuits [28] that are crucial building blocks in chip design for logic functions such as NAND, NOR, and NOT. The most basic component for these circuits is the voltage inverter, which inverts the incoming signal into an outgoing signal. CMOS inverters in silicon-based technology are composed of a p-type and an n-type transistor. As we will discuss in the following paragraphs, also bipolar transistors can be used for the purpose. Figure 16.6a shows the schematic of a complementary inverter [16]. In operation, the p- and n-type transistors are connected at the drain and the gate electrodes serving as output ($V_{out}$) and input ($V_{in}$) nodes, respectively. The source of the load transistor is connected to the power supply ($V_{supply}$), while the source of the driver transistor is grounded. The state of the n- and p-type transistors can be varied by changing the input voltage. An example of the quasi-static transfer curves of an inverter is shown in Figure 16.6b where a sharp inversion of the input signal can be observed with the maximum voltage gain [16]. An important characteristic of complementary inverters is that when the output is in a steady logic state ($V_{out} = 0$ or $V_{supply}$), only one of the transistor is "on" and the other is in "off" state. This reduces the current flow to a minimum equivalent to the leakage current through the transistor. Only during switching both transistors are "on" for a very short time. This considerably reduces the power consumption of these circuits with respect to other circuit architectures. Therefore, the advantages of

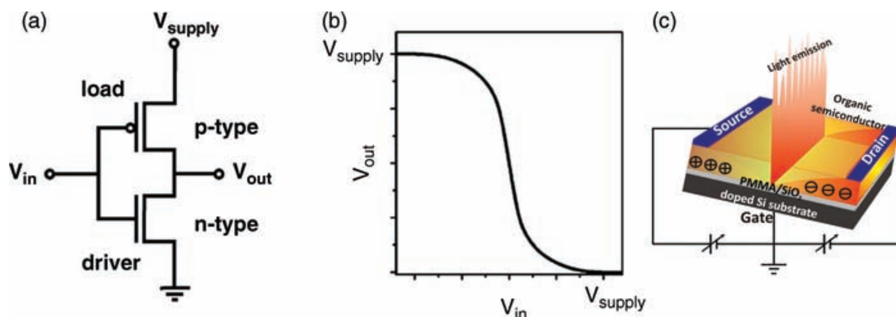


**Figure 16.6** (a) Illustration of a complementary inverter structure. (b) Transfer characteristics of a voltage inverter. (c) Schematic of the LE-FET. (Reprinted with permission from Ref. [16, 20])

CMOS inverters are that they can operate at relatively high speed with very little power loss and exhibit good noise margins in both low and high states.

Light-emitting field-effect transistors combine the switching properties of transistors with the electroluminescence of light-emitting diodes. They have been demonstrated recently for several classes of materials including inorganic semiconductors [29], carbon nanotubes [30], and organic semiconductors. LE-FETs provide planar nanometer-sized light sources that can be easily integrated in silicon, glass, or plastic substrates. Organic semiconductors often show strong photoluminescence [31] and electroluminescence [32], making them ideal active layers for this new class of devices. LE-FETs can be realized by using a p–n junction within the transistor channel forming a radiative recombination interface for electrons and holes. The requirements for good performing LE-FETs are: (i) balanced electron and hole mobilities, (ii) control over the position of the recombination zone, (iii) high current densities. Figure 16.6c shows a schematic of the LE-FET and its working mechanism [33].

## 16.3 Bipolar Field-Effect Transistors

### 16.3.1 Single-Component Bipolar FETs

From the electronic point of view organic semiconductors should in principle conduct equally both positive and negative carriers. However for many years the vast majority of known organic semiconductors have displayed either positive (p-channel) or, in smaller number, negative (n-channel) transport properties. Recently, the crucial role played by traps for the electron current has been understood. These traps are present as impurities of the semiconductor and on the surface of several dielectrics commonly used in the fabrication of FETs (hydroxyl, silanol, and carbonyl groups). Therefore, only with an appropriate treatment of the dielectric surface and by using pure materials processed in an inert atmosphere, it was possible to observe electron transport in several polymers, previously considered only p-type [34]. The use of bipolar materials allows for the fabrication of complementary-like circuits through the use of a single component that functions both as p-channel and/or as n-channel. This significantly reduces fabrication complexity avoiding the necessity of micropatterning of the p-channel and n-channel.

A challenge in fabricating ambipolar transistors from a single component consists in getting efficient injection of both charge carriers from the same electrode. Optimal charge injection takes place when the work function of the metal electrode lines up with the HOMO level of the semiconductor for hole injection and with the LUMO level for electron injection. Since most of the standard organic semiconductors have band gaps of 2–3 eV, the injection of at least one carrier will be contact limited for any given electrode material. However, one may also consider realizing asymmetric electrodes by choosing two different materials for each contact.

Separately engineering distinct contacts for hole–electron injection in bipolar OFETs will facilitate more efficient injection of the two types of carriers, but at the same time it will make the device realization more complex.

The issue of the injection for the same metal can be solved by using polymer with a narrow band gap (i.e., lower than 1.8 eV). This lowers the injection barrier for both charge carriers and efficient ambipolar transport can take place. This concept was first demonstrated by Klapwijk and coworkers [13], who investigated a few wide-band gap polymers, (poly[2-methoxy-5-(3′,7′-dimethyloctyloxy)]-*p*-phenylene vinylene (OC1C10-PPV) and related PPVs, poly(2,5-thienylene vinylene) (PTV), and P3HT) and attributed the lack of ambipolar transistor action to the presence of large injection barriers. To confirm this point they reduced the barrier using a small bandgap polymer, poly(3,9-di-*t*-butylindeno[1,2-b] fluorene) (PIF), which has a band gap energy of 1.55 eV. Typical output characteristics of a field-effect transistor based on PIF in combination with gold electrodes demonstrated operation both in the hole-enhancement mode and in the electron-enhancement mode. They also pointed out that the purity of the material is an important requirement to achieve ambipolar operation.

The same concept was further investigated by Sirringhaus and coworkers [35] who synthetized a series of regioregular polyselenophene-based polymers, which, with respect to polythiophene, present a reduced band-gap. The lower lying LUMO in these polymers results in an improved electron transport due to an enhanced electron injection from the metal electrodes and to reduced susceptibility of electrons to traps states and oxidation. Top-gate, bottom contact (TG/BC) transistor configurations with gold source–drain electrodes were used for all polymers. The best polymer, poly(3,3″-di-*n*-decylterselenophene) (PSSS-C10) showed clean ambipolar transport characteristics with similar hole and electron saturation and linear mobilities of $>0.01\ \mathrm{cm^2\ (V^{-1}\ s^{-1})}$ (PMMA as gate dielectric) (Figure 16.7a). While the saturation mobility values for holes and electrons were similar, some reversible hysteresis was systematically observed in the transfer characteristics in the electron transport regime but not in the hole transport regime, thus indicating the presence of a larger number of shallow traps for electrons than for holes. This is a common issue in bipolar semiconductors, which makes the observation of n-type regime more difficult and in general limits the value of the electron mobility. Using this polymer, complementary-like inverters based on two identical TG/BC ambipolar transistors were fabricated, with a common gate as input and a common drain as output, eliminating the need for semiconductor patterning. Despite the general fact that none of these TFTs can be fully switched off, the authors obtained very high switching gain in this inverter, with an absolute value as high as 86 (Figure 16.7b). This is one of the higher gain values reported so far in inverters composed of bipolar organic FETs.

For the realization of narrow band gap polymers, a useful synthetic strategy consists in copolymerizing an electron-rich and an electron-poor unit, to obtain a donor–acceptor structure. An example of this alternating donor–acceptor architecture has been reported by Jenekhe [36] with the synthesis of the copolymer PNIBT consisting of an electron-donating dialkoxybithiophene and

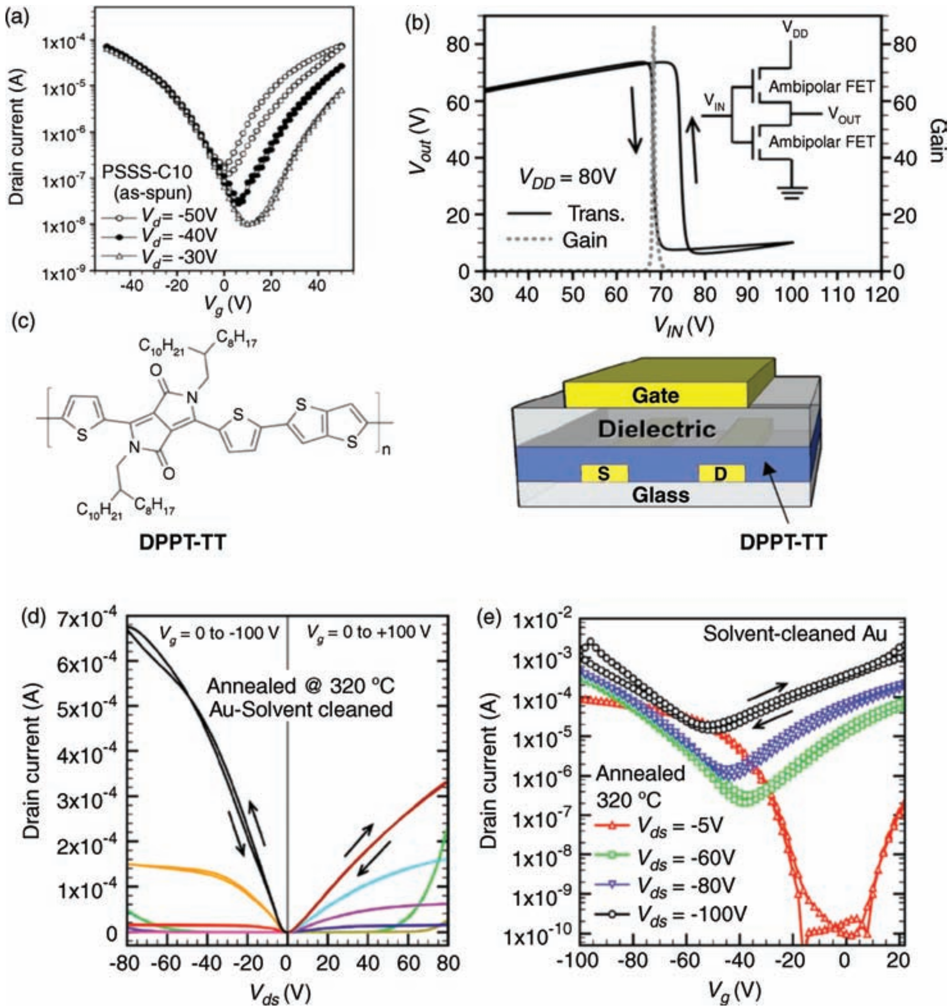


**Figure 16.7** (a) Transfer characteristics of an as-spun PSSS-C10 ambipolar FET with channel length ($L$) of 40 μm and channel width ($W$) of 2 cm. The hole and electron mobilities for this device are both ∼0.026 $cm^2$ ($V^{-1}\,s^{-1}$). (b) The transfer characteristic and the corresponding gain (in absolute value) of a complementary-like inverter comprises two identical as-spun PSSS-C10 TG/BC ambipolar FETs. The inset shows the inverter circuit configuration. (c) Chemical structure of the DPPT-TT polymer and schematic diagram of the top gate, bottom contact OFET structure. The output and transfer (d and e) characteristics of a typical OFET based on DPPT-TT thin films annealed at 320 °C. (Adapted with permission from Ref. [35]).

electron-accepting naphthalene bisimide. High-mobility ambipolar transistors and high-gain complementary-like inverters were fabricated and exhibit electron and hole mobilities as high as 0.04 and 0.003 $cm^2$ ($V^{-1}\,s^{-1}$), respectively, and output voltage gains as high as 30.

In the previous example, and in most of the ambipolar polymers reported, there is an unbalanced charge transport, the hole mobility being always higher than the electron mobility. In order to solve this problem it is possible to either optimize the device or introduce a stronger electron withdrawing unit in the donor–acceptor structure of the polymer. Following this strategy to improve the electron transport characteristics, Cho *et al.* introduced a more deficient building block, benzothiadiazole (BZT), in the donor–acceptor alternating copolymer consisting of DPP and two unsubstituted thiophene rings [37]. The resulting polymer, PDTDPP-*alt* –BTZ, exhibits balanced hole and electron mobilities of 0.061 and 0.054 $cm^2$ $(V^{-1} s^{-1})$, respectively. These values were obtained using a bottom gate, top contact configuration with Ag source–drain electrodes. The authors observed that when different work function metals were used as the source and drain electrodes, it was possible to improve the n-type and p-type performances. The mobilities obtained from the optimized FET with two different electrodes (Au for source electrode and Al for drain electrode) were 0.097 $cm^2$ $(V^{-1} s^{-1})$ for the hole and 0.089 $cm^2$ $(V^{-1} s^{-1})$ for the electron. The well-balanced bipolar nature of PDTDPP-*alt* –BTZ FETs makes the materials suitable for the realization of CMOS-like inverters. The steepness of the inverter curve indicated the maximum gain of $\sim$35, which is a relatively good value for single-component-based inverters fabricated from organic semiconductors.

This demonstrates that an accurate design of the polymers combined with a careful optimization of the device architecture, charge injection, and thin film quality enable to reach high, balanced electron and hole mobilities. A further improvement in the device performance has been reported by Sirringhaus and coworkers with the synthesis of a diketopyrrolopyrrole polymer, DPPT-TT (Figure 16.7c), with balanced hole and electron field-effect mobilities both exceeding 1 $cm^2$ $(V^{-1} s^{-1})$ [11]. The narrow band gap and the position of the HOMO and LUMO energy levels were designed to enable efficient bipolar charge injection and transport. For the realization of the devices, the authors used a bottom contact top gate configuration with PMMA as dielectric. The drawback of this system is that in order to observe high electron mobility an annealing treatment of the devices at 320 °C was necessary. This treatment allows eliminating electron-trapping impurities in the DPPT-TT films and improves the contact of the polymers with the electrodes. After the optimization of the annealing temperature and the contact electrode functionalization, the authors realized a complementary-like voltage inverter by combining two identical ambipolar DPPT-TT OFETs with a common gate as the input voltage ($V_{in}$) and a common drain as the output voltage ($V_{out}$). The inverter static-voltage-transfer characteristic exhibited a good symmetry with a switching voltage nearly half of that of the power supply ($V_{DD}$), little hysteresis, and a relatively high gain (absolute value of gain $> 20$) comparable with previously reported complementary-like inverters based on bipolar OFETs. These results show that DPPT-TT based OFETs are promising candidates for applications in ambipolar devices and integrated circuits, as well as model systems for fundamental studies of bipolar charge transport in conjugated polymers. However, the high annealing temperature required to reach high electron mobility is a limiting factor for the application and

implementation in circuit. Research is therefore focused on synthesizing polymers that can provide balanced bipolar behavior, with high hole and electron mobility, at room temperature.

In a similar system, Winnewisser and coworkers investigated the possibility to combine both ambipolar behavior and light-emitting properties [38]. They reported on a narrow band gap diketopyrrolopyrrole-based polymer, BBTDPP1, with ambipolar charge transport properties and near-infrared light emission from top-gate as well as bottom-gate transistor structure. By recording the electroluminescence with an infrared sensitive camera system, they showed that the recombination zone is moving through the transistor channel. This is an indication that the transistor is working in a truly bipolar mode: both a hole and an electron accumulation layer coexist and recombination occurs at the point in the channel where the two meet, depending on the relative gate and source drain voltage applied.

### 16.3.2 Bilayer Bipolar FETs

The possibility to obtain bipolar behavior in organic field-effect transistors by combining layers of n-type and p-type materials was first demonstrated in systems where both layers were deposited by evaporation. Dodabalapur and coworkers combined layers of two small molecules, the hole-conducting R-hexathienylene (R-6T) and the electron-conducting fullerene $C_{60}$, and observed both hole and electron transport in these devices, although with lower mobilities than those of the single component [39]. Both the relative position of HOMO and LUMO levels of the two materials as well as the deposition order were found to be important for achieving bipolar characteristics. Using this approach different combinations of hole conducting and electron conducting small molecules have been explored [40–42]. Air-stable, ambipolar transistors based on copper-hexadecafluoro-phthalocyanine (FCuPc), as an efficient electron conductor, and 2,5-bis(4-biphenylyl)-bithiophene (BP2T), as a hole conductor, were reported by Wang *et al.* Figure 16.8 shows the output (a) and transfer (b) characteristics of such a device. Using this material combination, bipolar mobilities of up to $0.04\,cm^2\,(V^{-1}\,s^{-1})$ for holes and $0.036\,cm^2\,(V^{-1}\,s^{-1})$ for electrons are possible under ambient conditions. Inverters fabricated with these transistors showed gains as high as 13 and good noise margins [43].

Dinelli *et al.* showed that by using layered structures of small molecules it is also possible to obtain light emission together with balanced ambipolar transport. For this application, α,ω-dihexyl-quaterthiophene (DH4T) and *N,N*′-ditridecylperylene-3,4,9,10-tetracarboxylic diimide (P13) were used for the p- and n-type layers, respectively (Figure 16.8c). The mobility values reported are as large as $3 \times 10^{-2}\ cm^2\,(V^{-1}\,s^{-1})$, among the highest values reported for bipolar bilayer OLETs. Morphological analysis by confocal PL microscopy indicates that "growth" compatibility is required in order to form a continuous interface between the two organic films. The authors pointed out that this compatibility is crucial in controlling the quality of the interface and the resulting optoelectronic properties of the OLETs. Therefore, they concluded that the optimum performance is not necessarily achieved by

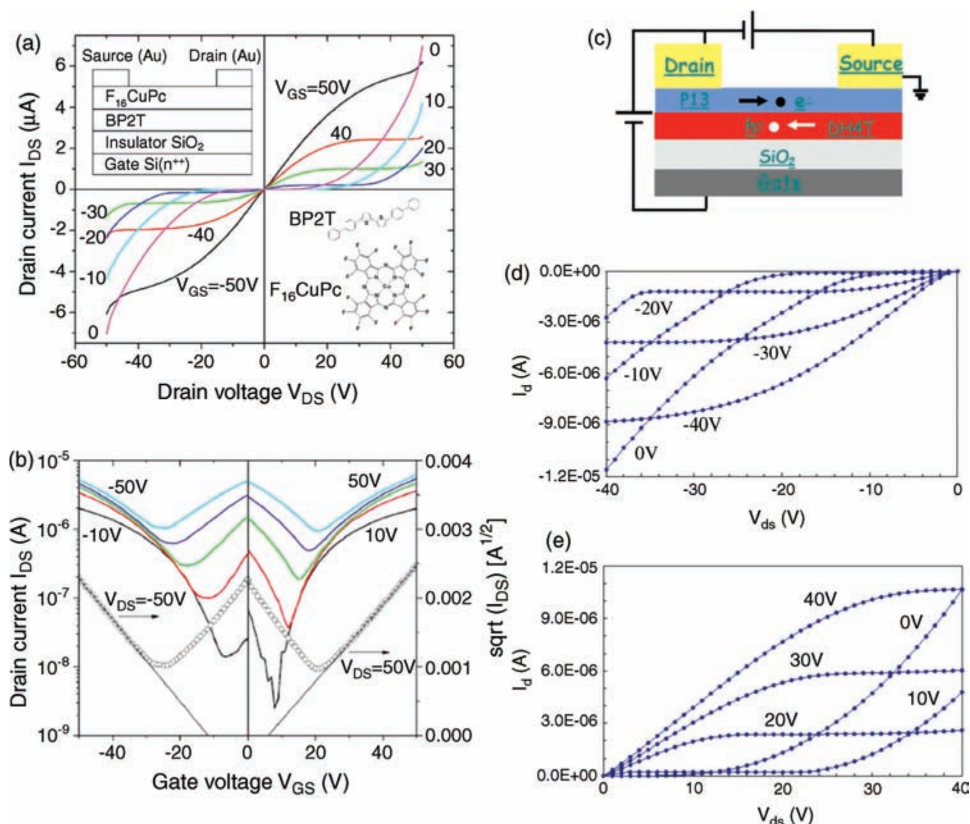


**Figure 16.8** (a) Typical output characteristics of bipolar OFETs based on FCuPc and BP2T bilayers for positive and negative gate biases. A schematic cross-section of the device structure and the molecular structures of FCuPc and BP2T is given in the insets. (b) Typical transfer characteristics for positive and negative gate biases. The solid lines show the logarithmic drain current versus gate voltage for various $V_{ds}$, and the open symbols show the square root of the drain current. (c) Schematic of an OLET device based on a DH4T–P13 bilayer. (d) Output curves ($I_d$ vs. $V_{ds}$) obtained from a DH4T–P13 device operating in a p-type configuration or in an n-type configuration. $V_{gs}$ values are reported beside each curve. $I_d$ = drain current; $V_{ds}$ = drain–source voltage; $V_{gs}$ = gate–source voltage. (Reprinted with permission from Ref. [43]).

employing materials with the highest mobility values in the single-layer devices, but by combining materials that are compatible and able to form a defined interface when evaporated one on top of the other [44].

In the bilayer architecture, depending on the device configuration and on the materials used, charge accumulation and transport of holes and electrons can occur in different layers. However, at least one of the two accumulation zones will form at the interface between the two organic layers and therefore charge transport will depend on the quality of this interface. In bilayer devices realized by evaporation,

as shown in the previous examples, an accurate control of the growth conditions is necessary. In order to reach balanced bipolar behavior, intermixing between the two layers and rough interfaces need to be avoided, since they limit charge transport. This is the reason why almost all the examples of bilayer ambipolar transistors are based on sublimed small molecules thin films. There are very few reports on bipolar bilayer transistors based on solution-processed semiconductors [45, 46]. This is due to the well-known difficulty in fabricating well-defined smooth bilayer structures by depositing one component on top of the other, without damaging the layer underneath and without intermixing. A possible solution to this issue has been proposed by Heeger *et al.* who realized FETs using regioregular poly(3-hexylthiophene) (rr-P3HT) and [6,6]phenyl $C_{61}$ butyric acid methyl ester (PCBM) separated by an intermediate layer of titanium oxide ($TiO_x$). All layers were processed from solution. In this multilayer FET structure, the $TiO_x$ layer enables the bipolar properties by electronically separating the p- from the n-channel. The comparison of the data with and without the $TiO_x$ confirms its role as an electron transport and hole blocking material. The optimized device shows good hole and electron mobilities, $8.9 \times 10^{-3}$ cm$^2$ (V$^{-1}$ s$^{-1}$) in the *n*-channel mode and $5.7 \times 10^{-3}$ cm$^2$ (V$^{-1}$ s$^{-1}$) in the p-channel mode [47].

An alternative approach for the realization of bipolar organic thin-film transistors with a bilayer structure has been demonstrated by Hashimoto and coworkers by using a contact-film-transfer method. They successfully fabricated bipolar FET and inverters based on a bilayer structure of P3HT and PCBM using a simple solution-based, contact-film-transfer method (Figure 16.9a). The transistors exhibited balanced electron and hole mobilities of $2.1 \times 10^{-2}$ and $1.1 \times 10^{-2}$ cm$^2$ (V$^{-1}$ s$^{-1}$), respectively. Complementary inverters based on two identical bipolar transistors showed good performance with a gain of 14 (Figure 16.9d). These results indicate that the contact-film-transfer method provides a facile way to construct multilayered structures with well-defined smooth interfaces and to fabricate complex organic electronic devices. The authors pointed out that further improvement could be achieved by using other organic materials with higher mobilities [48].

Jenekhe and coworkers demonstrated the possibility to obtain well-defined n–p polymer–polymer heterojunctions for bipolar FETs using sequential spin coating from solutions. By selecting polymers soluble in orthogonal solvents, it was possible to deposit one directly on top of the other, without using film transfer and lamination [12]. The polymer used for the n-type layer poly(benzobisimidazobenzophenanthroline), BBL, is soluble in methane sulfonic acid but not in chlorinated aromatic solvents whereas the p-type polymers P3HT, poly(benzobisthiazole-*alt*-3-octylquarterthiophene) PBTOT, and poly(thiazolothiazole) PSOTT are soluble in the latter solvents (Figure 16.10a). Bipolar charge transport in the n–p heterojunctions had electron and hole mobilities of ~0.001–0.01 cm$^2$ (V$^{-1}$ s$^{-1}$), which are similar to those measured in the corresponding single-layer OFETs. This demonstrates that the deposition of the second layer does not affect the performance of the first one. The authors also tracked the field-effect mobilities of electrons and holes in the n–p heterojunction FETs in air for more than 6 months recording good stability (Figure 16.10d).

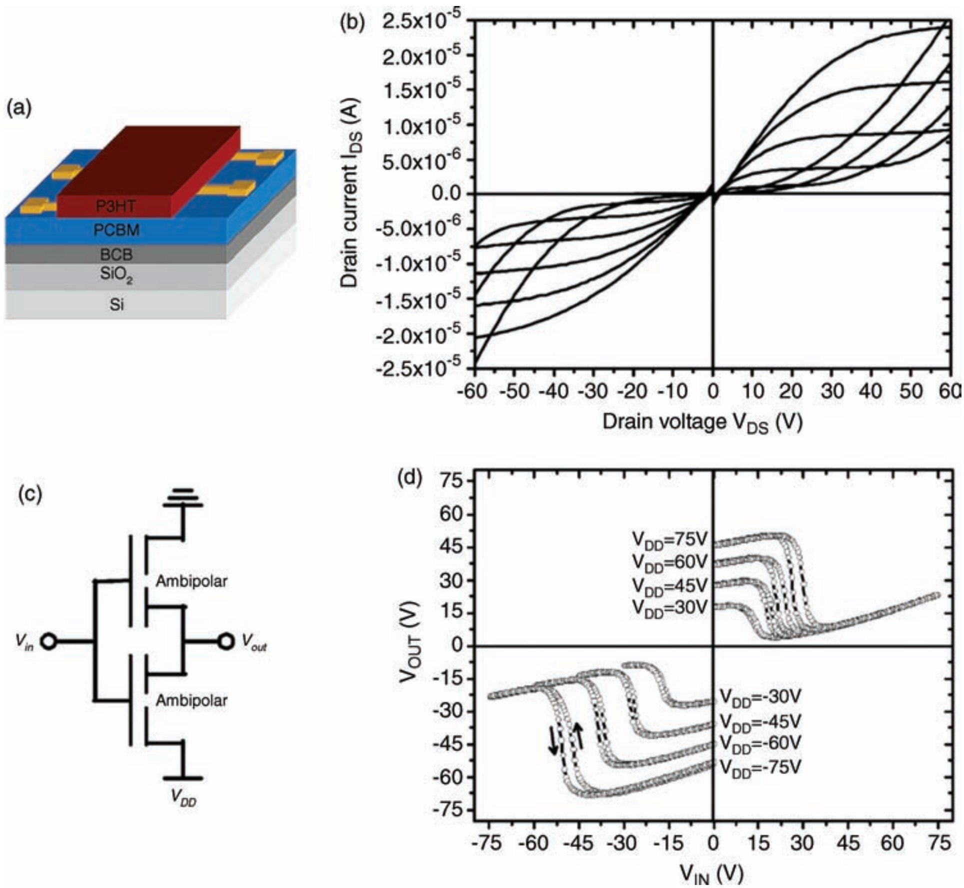


**Figure 16.9** (a) Schematic structure of the bilayer realized by contact-film-transfer method. (b) Output characteristics of the P3HT/PCBM bilayer transistor. (c) Schematic representation of the electrical connections for the inverter based on two identical ambipolar transistors and (d) transfer curves. (Reprinted with permission from Ref. [48]).

Moreover, the authors showed the application of these devices in logic circuits. Digital logic circuits that perform a logic calculation of binary information (represented by 0 and 1) have played an essential role in the development of current information technology. These circuits are fabricated by integration of multiple field-effect transistors. Sharp signal switching of the circuits can be obtained from complementary circuits that consist of p- and n-type transistors or bipolar transistors. Each transistor is selectively turned on and off based on the voltages at the terminal electrodes, inducing current flow through a certain pathway of the circuit and resulting in the targeted output voltage, which is close to either the supplied voltage ($V_{dd}$; representing signal 1) or ground (representing signal 0) of the logic operation. For example, the input signal is inverted after NOT gate operation (from 0 to 1, or from 1 to 0). The output signal of NAND gate is 0 only when two input signals are 1;

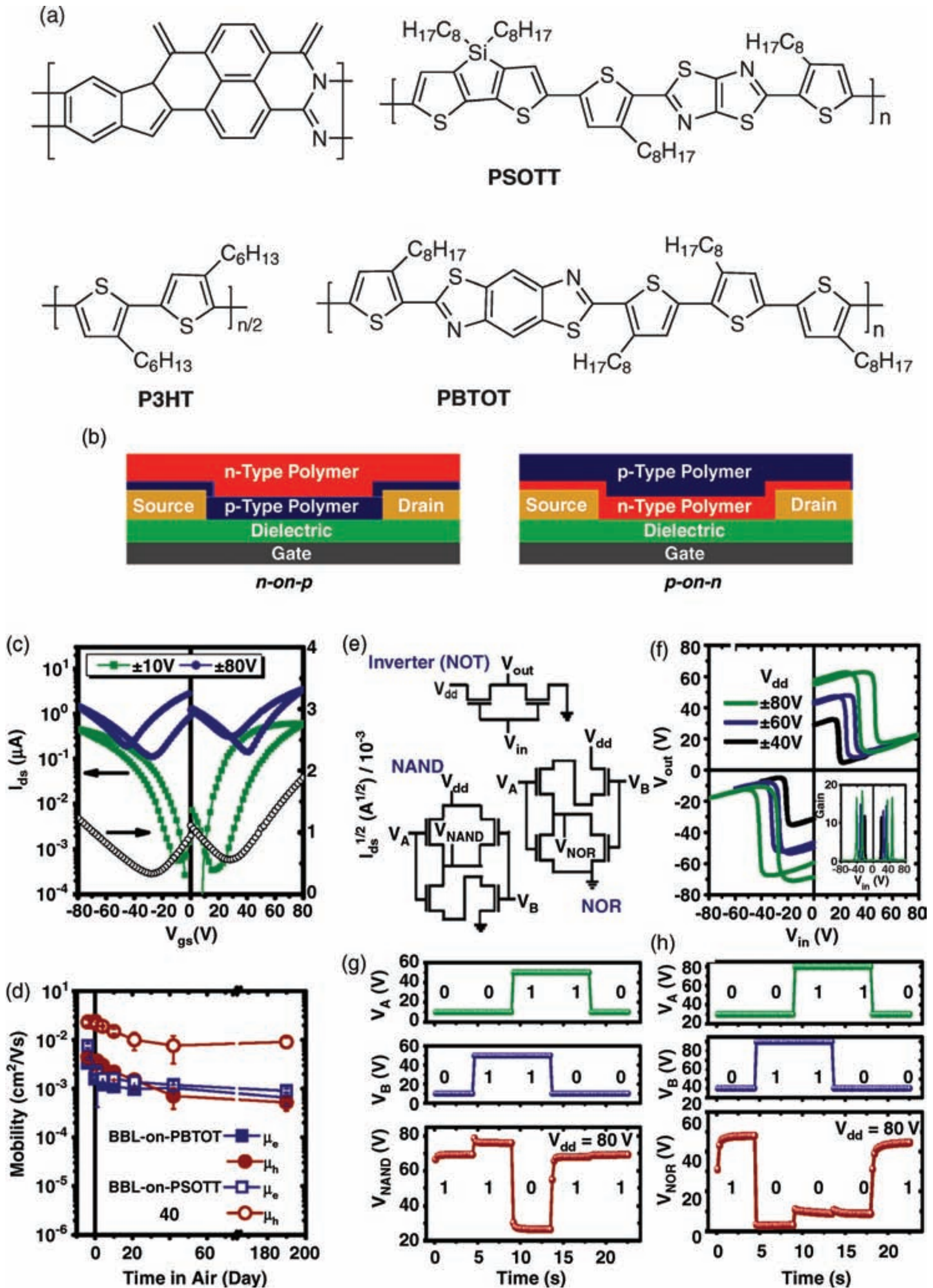


**Figure 16.10** (a) Molecular structures of the n-channel (BBL) and p-channel polymer semiconductors (P3HT, PBTOT, and PSOTT). (b) Schematics of bipolar field-effect transistors based on n/p polymer heterojunctions. (c) Transfer curves of a BBL-on-PBTOT bilayer

otherwise the output is 1. The NOR operation results in 1 only when the input signals are both 0. Complementary NOT gate requires one n-channel transistor and one p-channel transistor, and complementary NAND and NOR gates require two n-channel transistors and two p-channel transistors each. The advantage of using bipolar transistors in logic gate is that it is possible to use one type of transistor, although the total number of transistors is the same as in circuits with unipolar transistors (Figure 16.10e). Circuit diagrams of an inverter (NOT-gate) consisting of two transistors, and two-input NAND and NOR circuits with four transistors each, are shown in Figure 16.10e. The circuits consist of identical bipolar FETs from BBL-on-PBTOT n–p heterojunctions with the same geometric factors.

Complementary logic gates, including NOT, NAND, and NOR circuits, based on the polymeric bilayer bipolar OFETs exhibited sharp switching, with a gain as high as 16–18 (Figure 16.10f). Some degree of hysteresis is likely due to the threshold voltage difference of n- and p-channel modes in the individual OFETs. In the logic circuits of NAND and NOR gates, good switching characteristics were also observed, as shown in the output voltages plotted with the corresponding input voltages $V_A$ and $V_B$ (Figure 16.10g and h). High and low voltages at the terminals represent signals 1 and 0, respectively. These results demonstrate that bipolar OFETs can be used for designing and constructing various complementary circuits. Because bipolar transistors and circuits are fabricated by simple solution process, the devices presented here could ultimately be printable allowing for the effective use of this approach on a large area.

### 16.3.3 Bulk Heterojunction Bipolar FETs

Another way to obtain bipolar performance is to blend n- and p-type organic semiconductors, combining the advantageous properties of the two components in a single structure. Blending organic materials may lead to heterostructured bipolar FETs when an interpenetrating (percolation) network of the two materials is obtained. This can be achieved by coevaporation or solution processing, if the two materials are soluble in a common solvent.

In comparison to single-component films, bipolar semiconducting blends are much more challenging. The necessity to have percolation networks for both electrons and holes, each one conducted by one component of the blend, imposes strict requirements for the supra-molecular organization of the two materials. On one side an extended intermixing of the two semiconductors at the molecular level will

transistor. (d) Hole and electron mobilities in the BBL on-PBTOT and BBL-on-PSOTT transistors as a function of time in air. Data points before day 0 represent the mobilities in inert conditions. (e) Circuit diagrams of a complementary inverter, and NAND and NOR logic gates. (f) Voltage transfer characteristics of an inverter. (g, h) Output voltages of complementary logic gates and the truth tables with corresponding input voltages $V_A$ and $V_B$: (g) NAND and (h) NOR gates. The transistors in the circuits are based on BBL-on-PBTOT heterojunctions. (Reprinted with permission from Ref. [12]).

be negative, since it will allow electron–hole recombination; and on the other side macroscopic phase segregation can determine low percolation of the carriers between source and drain electrodes and it can cause problems for the charge injection. In conclusion, the main challenge is controlling the phase separation degree between the two components of the blend during the deposition process. This can be achieved by warily tuning the processing temperature, the solution viscosity, and the evaporation rate of the solvent. The objective is to adjust the miscibility and degree of crystallinity of the individual compounds in order to obtain in the blend continuous percolation pathways for both electrons and holes.

#### 16.3.3.1 Coevaporated Blends

Although the bilayer approach yields some impressive device characteristics and interesting insight into the electronic properties of organic semiconductor interfaces, it is still an issue to deposit two layers one top of the other. Lamination and transfer methods are not compatible with printing technology and sequential depositions directly from solution are challenging due to the need of orthogonal solvents for the deposition of the two layers. An alternative method is to use blends of n- and p-channel materials to realize bipolar transport in a single layer. For the blend approach, both coevaporated and solution-processed films are feasible.

Rost *et al.* showed that coevaporating *N,N*8-ditridecylperylene-3,4,9,10-tetracarboxylic diimide PTCDI-$C_{13}H_{27}$ (P13) and quinquethiophene (5T) (Figure 16.11a),

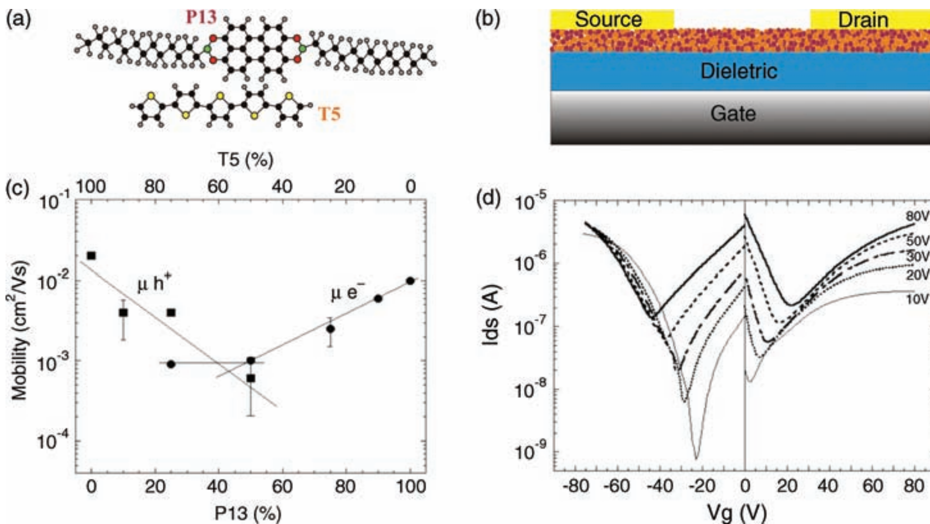


**Figure 16.11** (a) Molecular structure of 5T and PTCDI-$C_{13}H_{27}$ and (b) device structure of bipolar field-effect transistor consisting of a coevaporated thin film of 5T and PTCDI-$C_{13}H_{27}$. (c) Electron (filled circles) and hole (filled squares) field-effect mobilities for different bulk-heterojunction compositions. (d) Transfer characteristics of the coevaporated 5T/PTCDI-$C_{13}H_{27}$ thin-film transistor for negative and positive gate biases. (Reprinted with permission from Ref. [21]).

with equal fractions results in good bipolar characteristics with hole and electron mobilities of $10^{-4}$ cm$^2$ (V$^{-1}$ s$^{-1}$) and $10^{-3}$ cm$^2$ (V$^{-1}$ s$^{-1}$), respectively, which were smaller than those for the pure materials [49]. This is understandable, as explained above, since in the blend there is an interpenetrating network of n-channel and p-channel materials. In the presence of a not optimized morphology of this network, electron–hole recombination may occur with consequent losses in carrier population. Despite these limitations, it is important to underline that this was the first report of a bipolar light-emitting transistor (LE-FET): the observation of pronounced ambipolar conduction over a wide range of bias conditions was accompanied by light emission.

Loi *et al.* later investigated the impact of the relative fractions of each material on hole and electron mobilities in the same system and found the expected increase of hole mobility with an increasing fraction of 5T and equally an enhanced electron mobility with an increasing PTCDI-$C_{13}H_{27}$ fraction (Figure 16.11c) [21]. Balanced hole and electron mobilities for this system are obtained with a ratio of PTCDI$C_{13}H_{27}$/5T of 2: 3. The authors were also able to detect electroluminescence from this system that correlates with the voltage applied at the drain–source and gate electrode. Moreover, by using laser scanning confocal microscopy, they found the relation between the working characteristics of the transistors (p-channel, n-channel, ambipolar) and the supra-molecular organization of the thin film. Other coevaporated blends resulting in bipolar transport include pentacene/PTCDI-$C_{13}H_{27}$ [50] and pentacene/fluorinated pentacene [51].

#### 16.3.3.2 **Polymer–Small Molecule Blends**

Due to the easy processing, thin films of solution processable polymer–small molecule composites are more appealing for the realization of integrated circuits on large area by printing techniques. As for the coevaporated systems, the composition and microstructure of the film will affect the performances of the devices. For the polymer–small molecule blends, these characteristics can be tuned by the choice of solvents and spin coating parameters [52], until the optimal conditions are reached for balanced bipolar transport.

The first bipolar FETs based on a blend were fabricated by Tada *et al.* [53, 54] by mixing the electron conducting dye *N*,*N*-bis(2,5-di-*tert*-butylphenyl)-3,4,9,10- perylene dicarboximide, whose chemical structure is similar to PTCDI-$C_{13}H_{27}$ (shown in Figure 16.11a), with p-type poly(3-dodecylthiophene) in chloroform and spin casting this mixture on a Si/$SiO_2$ substrate with prepatterned Ti/Au electrodes. Although bipolar behavior was observed, the effective mobilities were extremely low ($10^{-7}$ cm$^2$ (V$^{-1}$ s$^{-1}$) for holes and $10^{-9}$ cm$^2$ (V$^{-1}$ s$^{-1}$) for electrons).

The first demonstration of a polymer blend transistor with appreciable ambipolar mobilities was accomplished by Meijer *et al.* by blending poly(2-methoxy-5-(3,7-dimethyloctoxy)- *p*-phenylene vinylene) ($OC_1C_{10}$-PPV) and PCBM (Figure 16.12a) [13]. Here, the hole and electron mobilities reached $7 \times 10^{-4}$ cm$^2$ (V$^{-1}$ s$^{-1}$) and $3 \times 10^{-5}$ cm$^2$ (V$^{-1}$ s$^{-1}$), respectively. A representation of the interpenetrating network and cross-section of the field-effect transistor is presented in Figure 16.12a. For both materials the charge injection comes from

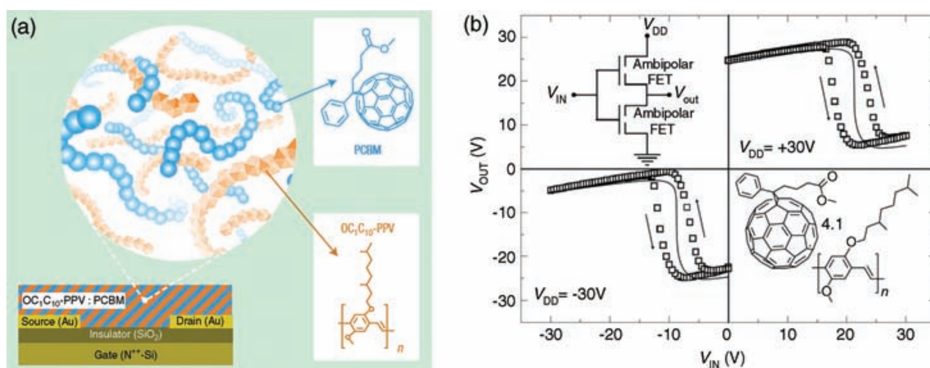


**Figure 16.12** (a) Schematic of the cross-section of the FET geometry; the molecular structures of PCBM and $OC_1C_{10}$-PPV and a representation of the interpenetrating networks of the two semiconductors. (b) Transfer characteristics of CMOS-like inverters based on two identical $OC_1C_{10}$-PPV: PCBM field-effect transistors. Depending on the polarity of the supply voltage, $V_{DD}$, the inverter works in the first or the third quadrant. A schematic representation of the electrical connections in the inverter is given in the inset. (Reprinted with permission from Ref. [13]).

the gold contact: the HOMO level of $OC_1C_{10}$-PPV, at −5.0 eV, is aligned with the work function of gold (about −5.1 eV), resulting in an ohmic contact for hole injection from gold into the $OC_1C_{10}$-PPV network. Instead the mismatch in energy levels between the gold work function and the LUMO level of the PCBM results in an injection barrier of about 1.4 eV for electron injection into the PCBM network. However, the authors claimed that this injection barrier can be significantly reduced to 0.76 eV, due to the formation of a strong interface dipole layer at the Au–PCBM interface.

Typical output characteristics of a field-effect transistor based on the $OC_1C_{10}$-PPV: PCBM blend, in combination with Au electrodes, demonstrated operation in both the hole-enhancement and electron-enhancement modes. For high negative $V_g$, the transistor is in the hole-enhancement mode and its performance is identical to a unipolar transistor based on $OC_1C_{10}$-PPV, with a field-effect mobility of $7 \times 10^{-4}\,cm^2\,(V^{-1}\,s^{-1})$. At positive $V_g$, the transistor operates in the electron-enhancement mode, with a field-effect mobility of $3 \times 10^{-5}\,cm^2\,(V^{-1}\,s^{-1})$. This mobility is two orders of magnitude lower than the electron mobility in a PCBM transistor [55] due to the interpenetrating network of the two components. For this kind of system, a better matching of the energy levels of the n-type semiconductors with the electrode metal work function could lead to a more balanced bipolar transport in the blend. Inverters based on two identical bipolar transistors were realized, demonstrating CMOS-like operation (Figure 16.12b). A gain of 10 for the $OC_1C_{10}$-PPV: PCBM blend inverter was easily achieved, in combination with a good noise margin.

Other examples of bipolar behavior have been reported for blends of poly(2-methoxy-5-(2c-ethylhexyloxy)-1,4- phenylenevinylene) (MEH-PPV) and $C_{60}$ [56],

MEH-PPV and PCBM [57], CuPc and poly(benzobisimidazo-benzophenanthroline) [58], and P3HT and PCBM [59].

The best results obtained until now with this class is reported by Shkunov *et al.* from bipolar blends of thieno[2,3-*b*]thiophene terthiophene polymer and phenyl $C_{61}$ butyric acid methyl ester (Figure 16.13) [27]. The authors studied the effect of different surface treatments and obtained the highest field-effect mobility for bipolar blends on OTS-treated substrates in saturation regime, with electron mobility reaching $9 \times 10^{-3}$ cm$^2$ (V$^{-1}$ s$^{-1}$) and hole mobility reaching $4 \times 10^{-3}$ cm$^2$ (V$^{-1}$ s$^{-1}$). CMOS-like inverters have been built on a single substrate using two identical transistors. As shown in the circuit schematic, a common gate has been used for both the transistors (inset in Figure 16.13c). The

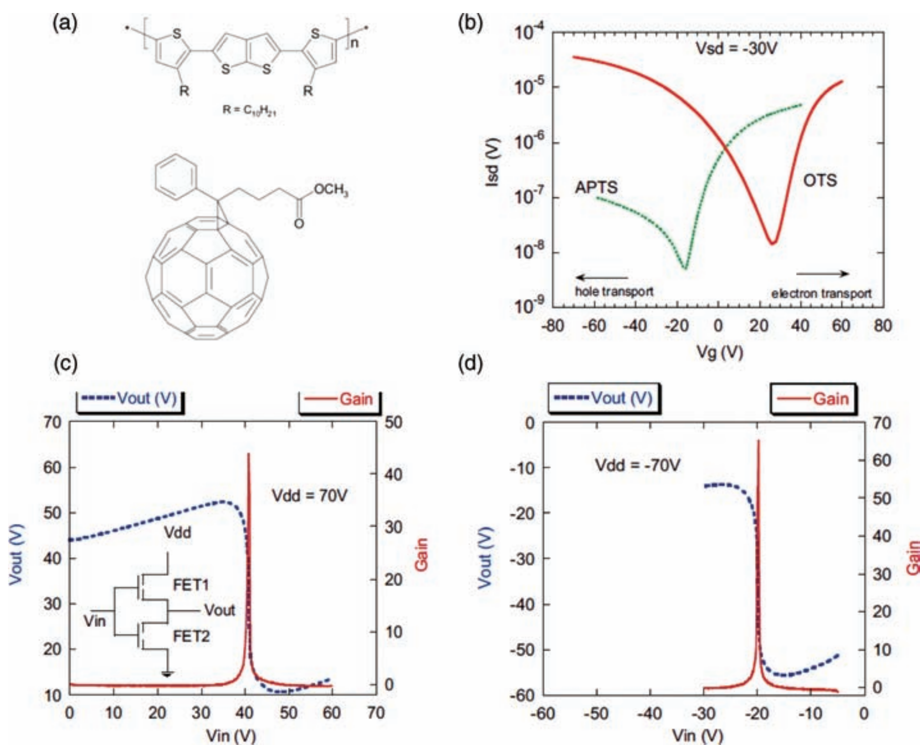


**Figure 16.13** (a) Chemical structures of thieno [2,3-*b*]thiophene terthiophene polymer and PCBM. (b) Transfer characteristics of FETs with APTS-modified (dotted line) and OTS-modified (solid line) $SiO_2$ surfaces. The polymer/PCBM blend composition is identical in both cases. The devices operated in electron-enhancement mode with offset voltages −16 and 27 V for APTS and OTS transistors, respectively. (c, d) Transfer characteristics of CMOS-like inverters are shown as dashed lines. The corresponding gain curves are thin solid lines. Inverters are operational in the first quadrant (d) or in the third quadrant (c). The inset of (c) shows the schematic configuration for these inverters based on two identical transistors. $V_{in}$: input voltage; $V_{out}$: output voltage; $V_{dd}$: supply voltage. (Reprinted with permission from Ref. [27]).

devices are operational in two quadrants: with positive supply ($V_{DD}$) and input ($V_{in}$) voltages, the inverters work in the first quadrant with a maximum gain of 45, whereas under negative bias, the inverters operate in the third quadrant and exhibit a gain of ~65, which is the highest value reported for inverters made with bipolar blends.

#### 16.3.3.3 **Hybrid Blends**

Reports on semiconducting polymer-inorganic material-based bipolar FETs are rare to date, most probably due to the difficulty in controlling the morphology of a complex active layer. Aleshin *et al.* have shown that embedding ZnO nanoparticles into poly[9,9-bis-(2-ethylhexyl)-9*H*-fluorene-2,7-diyl] (PFO) matrix can serve as active layer for light-emitting unipolar and bipolar transistors depending on the concentration ratio of the PFO:ZnO [60]. PFO is one of the most promising and widely used conjugated polymers for LEDs, while ZnO is a nontoxic, environmentally stable, and solution processable inorganic n-type semiconductor. Recently ZnO based FETs have been reported with very high mobilities up to 7.2 $cm^2$ $(V^{-1} s^{-1})$ in combination with high on/off ratio [61].

The major challenge in fabricating bipolar FETs arises from the mismatch of the electrode work function and the energy levels of the semiconductors. The authors have proposed to use two different metal electrodes to overcome this limitation. Gold electrodes have been used to inject holes into the HOMO levels of the PFO and aluminum electrodes to facilitate electron injection into the LUMO of the ZnO. Due to a large injection barrier, gold electrodes are unable to sufficiently inject electrons to the higher lying LUMO level of the ZnO.

The structure used for this device is composed of an n+ silicon substrate and 200 nm thermally grown $SiO_2$ as gate dielectric with thermally evaporated Au and Al electrodes. The device is finished by spin-casting or drop casting the blend of PFO and ZnO from chloroform with different concentration ratios. After deposition, the films were dried at 80 °C in $N_2$ for 15 min. The output and transfer characteristics of such a device are shown in Figure 16.14. The best results are produced with concentration ratio of 1: 0.2 between PFO and ZnO nanoparticles. The hole and electron enhancement modes are evident from Figure 16.14a and b. However, the characteristic S-shape of the output curves strongly suggests contact resistance problems. The transfer characteristic for the same device in Figure 16.14c shows both electron and hole accumulation regimes with a small reversible hysteresis. Electron and hole field-effect mobilities were found to be ~0.021 and ~0.029 $cm^2$ $(V^{-1} s^{-1})$, respectively. The on/off ratio for this device was calculated to be in the range of $\sim 10^3$ for $V_g \sim 20$ V. As the concentration of the ZnO nanoparticles increases the transfer plot of the PFO:ZnO FET becomes asymmetric indicating the transition to the n-type unipolar regime. The optical output characteristics (electroluminescence (EL) intensity versus $V_{ds}$) of the ambipolar PFO: ZnO FET, at different gate voltages, are shown in Figure 16.14d. The EL intensity is increasing by enhancing the source–drain voltage and both for negative and positive gate voltages. The onset of the light EL emission at $V_{ds} \sim -5$ V is nearly constant and independent of the ZnO nanoparticles concentration and the gate voltage polarity. The

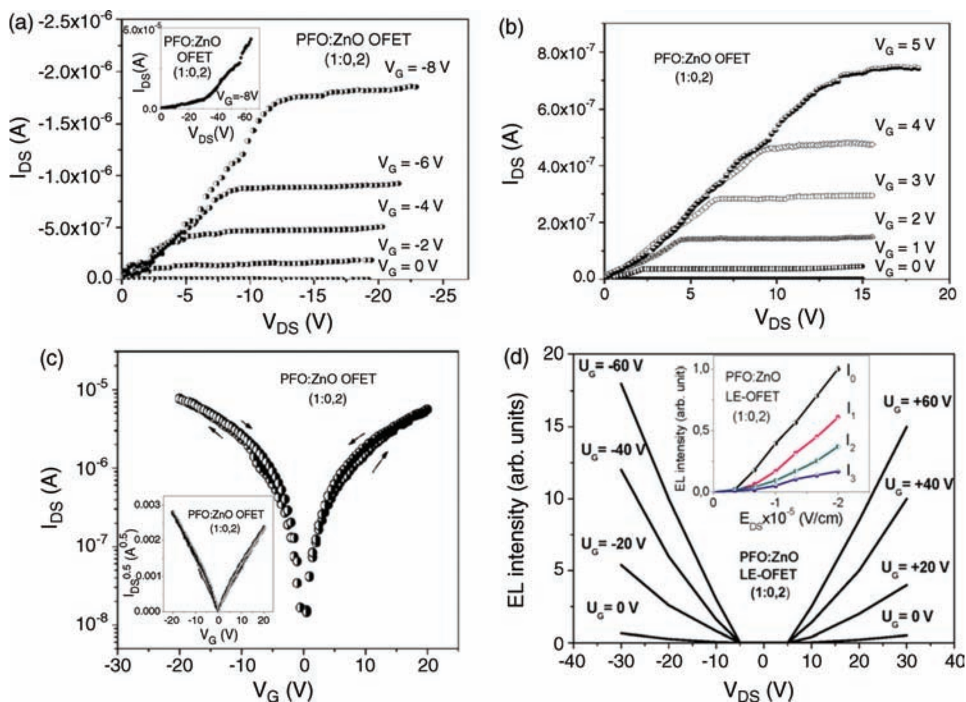


**Figure 16.14** (a) Output characteristics of the PFO:ZnO FET in hole enhancement mode; (inset) output $I$–$V$ characteristics for the same sample at high $V_{ds} > 20$ V and $V_G = -20$ V; (b) output characteristics in electron enhancement mode. (c) Transfer characteristic for $V_{ds} = -10$ V; (inset) square root of $I_D$ versus $V_g$ for the same sample; (d) EL intensity versus $V_{ds}$ at different $V_g$ (inset): EL intensity versus electric field for different spectral regions: $I_0$ – integral; $I_1$ – 600–830 nm; $I_2$ – 450–620 nm; $I_3$ – 300–400 nm. (Reprinted with permission from Ref. [60]).

inset in Figure 16.14d shows the EL intensity versus the electric field at different spectral regions. Clearly, the EL emission takes place mainly in the green spectral region and reaches ∼40% of the integral EL intensity, whereas in the blue region reaches only ∼20%. These results demonstrate that polymer composite thin films such as PFO and semiconducting nanoparticles can also serve as multifunctional devices fabricated by compatible techniques for printed technologies.

#### 16.3.3.4 **Polymer–Polymer Blends**

Blends of semiconducting polymers can also be used as active layers to achieve bipolar charge transport. Since controlling the morphology of polymer blends is challenging, there are only few reports based on polymer–polymer composite bipolar devices.

Babel *et al.* investigated the dependence of bipolar carrier transport on thin-film morphology [14]. They studied two series of binary polymer–polymer blends of the n-type poly(benzobisimidazobenzophenanthroline) (BBL) with the

p-type semiconductors poly[(thiophene-2,5-diyl)-*alt*-(2,3-diheptylquinoxaline-5,8-diyl)] ($PTHQ_x$) and poly(10-hexyl-phenoxazine-3,7-diyl-*alt*-3-hexyl-2,5-thiophene) (POT).

Atomic force microscopy (AFM) was used to investigate the thin-film blend morphologies of BBL/$PTHQ_x$ blend films as a function of the composition; the images are shown in Figure 16.15a. There are two distinct phases (lighter and darker) present in the images. The light features in Figure 16.15a correspond to $PTHQ_x$ since their size increases with increasing $PTHQ_x$ concentration. In the case of 10 wt% $PTHQ_x$ the phase-separated domain size is ~50 nm, which increases to ~300 nm in the 80 wt% $PTHQ_x$ blend. By increasing more the $PTHQ_x$ concentration, an interpenetrating two-phase bicontinuous network structure can be observed. These data were supported by transmission electron microscopy (TEM) measurements confirming that $PTHQ_x$ tends to form spherical aggregates randomly dispersed in the BBL matrix. The BBL/POT blends show similar phase separated morphology. The size of the light features increases by increasing the concentration of POT indicating the origin of this phase.

The compositional dependence of the charge transport was investigated in simple bottom contact/bottom gate FET configuration. The binary blends were spin coated from methanesulfonic acid (MSA) followed by drying and annealing in vacuum at 60 °C. Using 10–90 wt% $PTHQ_x$ in the BBL/$PTHQ_x$ blend, only

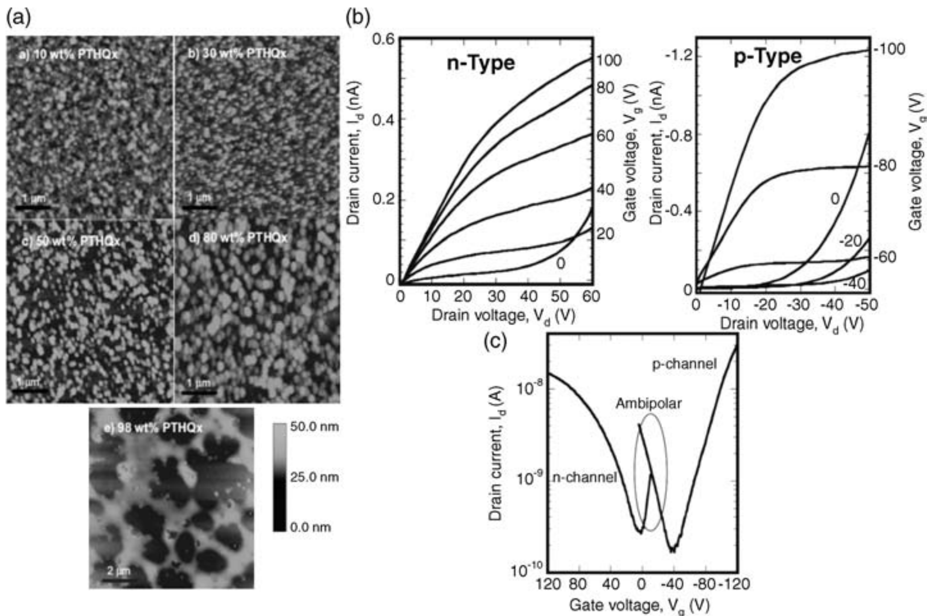


**Figure 16.15** (a) AFM topography images of 10, 30, 50, 80, and 98 wt% of BBL/$PTHQ_x$ blends. (b) Bipolar operation of the 98 wt% PTHQx blend in electron enhancement and hole enhancement mode. Transfer characteristics of a 98 wt% PTHQx blend. (Reprinted with permission from Ref. [14]).

unipolar electron transport could be observed. The calculated saturation field-effect electron mobility was relatively constant at $1.0 \times 10^{-3}\,cm^2\,(V^{-1}\,s^{-1})$ almost over the whole blend-composition range. It is interesting to note that the electron mobility did not decrease by adding the second component, if compared with the mobility in the BBL FET. In most of the cases the mobility sharply decreases by one or two orders of magnitude in the presence of another component in the active layer. However, when the $PTHQ_x$ concentration was increased to 90 wt%, a drop in the electron mobility was observed, indicating that the electron mobility in the BBL/$PTHQ_x$ blends is independent of the composition until a certain threshold in concentration is reached.

This constant electron mobility can be explained by considering the blend thin-film morphology. The AFM images show that even at high $PTHQ_x$ concentrations (50–80 wt%) $PTHQ_x$ exists as separate domains in the BBL matrix while BBL forms an interconnected matrix facilitating the electron transport. Since there is no sign of hole transport in these blends, it can be concluded that the single crystalline domains of $PHTQ_x$ are not connected. Ambipolar transport was observed in these blends only above 90 wt% $PTHQ_x$. The output and transfer curves of such a device are shown in Figure 16.15, where the 98 wt% PTHQx blend transistor operating in electron and hole enhancement mode is shown. At low gate voltages and high drain voltages the typical nonlinear increase in the drain current appears in both modes due to the formation of the p–n junctions in the channel. From the transfer curves, the saturation field-effect electron and hole mobilities were calculated to be $1.4 \times 10^{-5}\,cm^2\,(V^{-1}\,s^{-1})$ and $1 \times 10^{-4}\,cm^2\,(V^{-1}\,s^{-1})$, respectively. The hole field-effect mobility is still comparable to the single component $PTHQ_x$ device mobility, while the electron mobility in the blend at this concentration is about two orders of magnitude lower compared to the BBL-only device mobility. According to the authors, the decrease in the electron mobility of these bipolar FETs may be due to the smaller amount of BBL in the blend.

The BBL/POT blends showed similar trend: only electron transport was observed until a threshold concentration (50 wt%) of POT. Above this concentration bipolar transport appeared with electron and hole mobilities of $6 \times 10^{-4}\,cm^2\,(V^{-1}\,s^{-1})$ and $1.2 \times 10^{-6}\,cm^2\,(V^{-1}\,s^{-1})$, respectively for 80 wt% of POT. Both the electron and hole mobilities decreased in this blend with respect to the single-component devices, which can be explained by the variation of the morphology. The same authors investigated binary blends of poly(9,9-dioctylfluorene) and regioregular poly(3-hexylthiophene). The polymers were found to be phase separated and to exhibit only hole transport [62].

The lack of the bipolar transport in binary blends of polymers for most of the compositions shows that controlling the thin-film morphology is challenging. Therefore, the key issue is to realize an interpenetrating and bicontinuous networks of binary polymer blends in order to establish ambipolar charge transport.

Another example of all-polymer bulk heterojunction bipolar FETs was demonstrated recently by Szendrei *et al.* [15]. The limited number of polymer blend bipolar FETs is due to the scarcity of high-performing n-type polymers. The recent

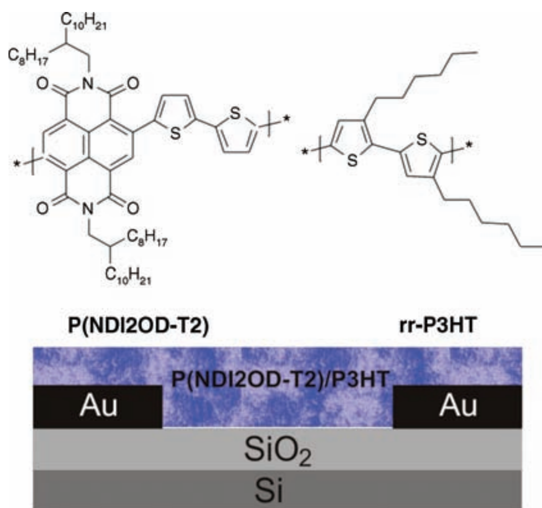


**Figure 16.16** Chemical structure of the semiconducting polymers P(NDI2ODT2) and rr-P3HT and illustration of the bottom-gate/bottom-contact bipolar FET architecture. (Reprinted with permission from Ref. [15]).

discovery of the n-type polymer poly{[*N,N′*-bis(2-octyldodecyl)-naphthalene-1,4,5,8-bis(dicarboximide)-2,6-diyl]-alt-5,5′-(2,2′-bithiophene)} (P(NDI2OD-T2)) [8] exhibiting large electron mobility in ambient conditions opened up the way toward the development of solution processed efficient polymer-based bulk heterojunctions. Using P(NDI2OD-T2) as the n-type component and regioregular poly(3-hexylthiophene) (rr-P3HT), the authors demonstrated a bipolar FET with high and balanced hole and electron mobilities. The chemical structures of P(NDI2OD-T2) and P3HT are shown in Figure 16.16, together with the device configuration used in this study to test the electrical properties of the polymer blend. The devices are fabricated in a bottom gate/bottom contact (Au) configuration where the polymer blend (typically in the proportion of 1 : 1 by weight) is spin coated from 1,2-orthodichlorobenzene (ODCB) and annealed overnight at 110 °C in a vacuum oven.

Figure 16.17 shows the output characteristics of the all-polymer bulk heterojunction FETs. The ambipolar nature in both electron enhancement (Figure 16.17a) and hole enhancement (Figure 16.17b) modes is evident. At high positive gate voltages ($V_g$) these transistors function as only electrons are accumulated at the semiconductor–insulator interface, similarly to the unipolar P(NDI2OD-T2) FETs. For lower $Vg$ the devices show the typical nonlinear increase in current at high $V_{ds}$ due to the injection of both charge carriers in the channel. However, at low $V_{ds}$ the output curves show clear indications of contact resistance for electron injection due to the injection barrier between the gold electrodes and the LUMO level of P (NDI2OD-T2).

A similar behavior is observed for hole transport when applying negative $V_g$ and $V_{ds}$ biases (Figure 16.17b). However, the current is far less limited for hole

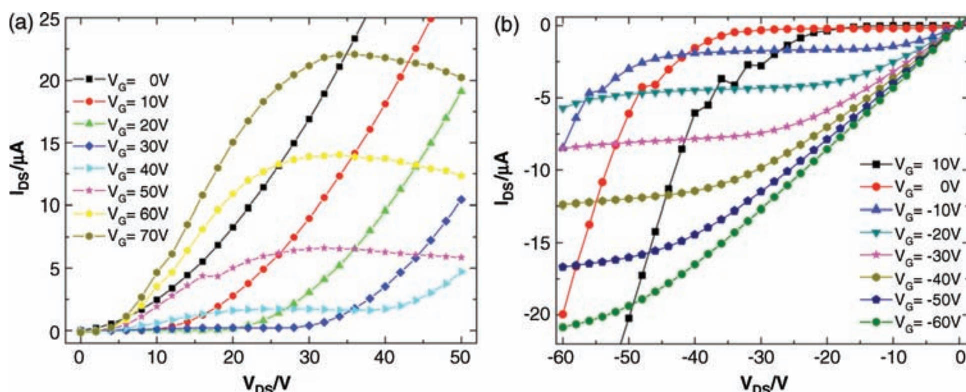


**Figure 16.17** Typical output characteristics of the bipolar polymer blend FETs in (a) electron enhanced mode and (b) hole enhancement mode. (Reprinted with permission from Ref. [15]).

injection due to the almost ohmic nature of the contact between Au and the HOMO level of rr-P3HT.

Figure 16.18a and b shows the transfer characteristics of these polymer bipolar FETs for positive and negative $V_{ds}$, respectively. In both cases the transfer shows a symmetric shape indicating the presence of balanced electron and hole populations in the channel. The saturation field-effect electron and hole mobilities were calculated to be $4 \times 10^{-3}\,cm^2\ (V^{-1}\,s^{-1})$ at $V_{ds} = +30\,V$ and a p-type mobility of $2 \times 10^{-3}\,cm^2\ (V^{-1}\,s^{-1})$ at $V_{ds} = -30\,V$. These mobilities are the highest balanced mobilities reported so far for solution processed all polymer bulk heterojunction bipolar FETs. The balanced FET mobilities indicate the presence of sufficient percolation pathways for both charge carriers in these polymer blends.

To provide evidence for the presence of good interpenetrating bicontinuous network, the surface morphology of the blend was investigated by AFM. Figure 16.19

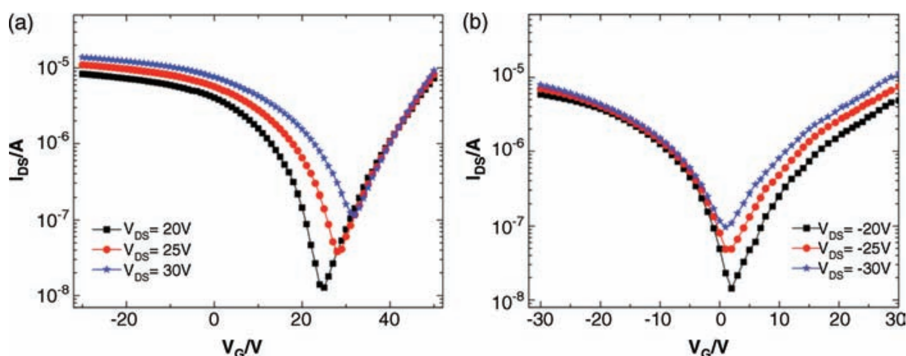


**Figure 16.18** Typical transfer characteristics of the bipolar polymer blend FETs in (a) electron enhancement mode and (b) hole enhancement mode. (Reprinted with permission from Ref. [15]).

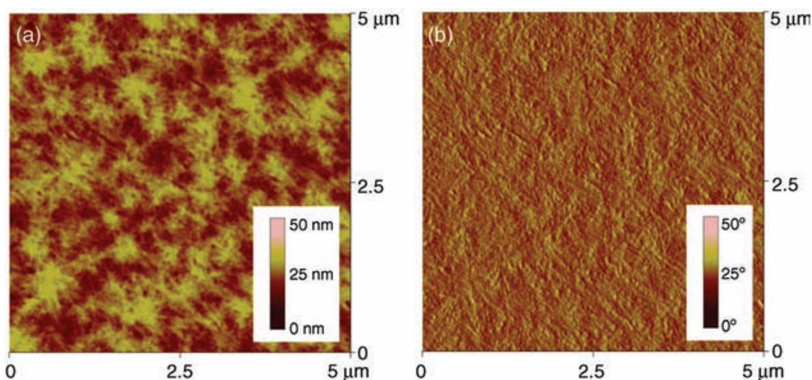


**Figure 16.19** AFM (a) topography and (b) phase images of the P(NDI2OD-T2)/rr-P3HT blends. (Reprinted with permission from Ref. [15]).

shows the AFM topography (a) and phase (b) of the P(NDI2OD-T2)/rr-P3HT active layer. The P(NDI2OD-T2)/rr-P3HT blend thin-film surface is quite smooth, characterized by small protrusions and an RMS roughness of 3.9 nm. The phase image (Figure 16.19b) shows a very fine network of the two materials with two different phases, suggesting phase segregation between P(NDI2OD-T2) and rr-P3HT. This fine network proves the presence of efficient percolation pathways for both charge carriers, supporting the good bipolar nature of this polymer–polymer blend.

Despite the challenge of controlling the morphology of polymer composite the excellent bipolar performance of these blends may hold promise for easy, cheap, and solution-processed bipolar optoelectronic applications.

## 16.4
## Perspectives

In this chapter we have reviewed the state of art in the fabrication of bi-polar field effect transistors by using different approaches. We have observed that, in the past few years, the synthesis of polymers with bi-polar characteristics has progressed considerably, also thanks to the understanding of the detrimental role of impurities and trapping (especially electron trapping) at the semiconductor–oxide interface.

A better understanding of the role of the supra-molecular order for the realization of continuous percolation paths for both charge carriers has brought noticeable improvement in the performances of polymer–polymer composites. Further improvements with this last approach will be achieved when methods for the control of the composite morphology will be developed. Moreover, the synthetic efforts toward better n- and p-type polymers will also be fundamental in the achievement of high bipolar mobilities and on–off ratios in polymer-based composites. In the meantime, it is possible that interesting results will come from emerging fields, as the organic–inorganic hybrid composites.

## References


1 Lilienfeld, E.J. (1928) US patent 1900018.
2 Horowitz, G. (1998) *Adv. Mater.*, **10**, 365–377.
3 Voss, D. (2000) *Nature*, **407**, 442–444.
4 Rotzoll, R., Mohapatra, S., Olariu, V., Wenz, R., Grigas, M., Dimmler, K., Shchekin, O., and Dodabalapur, A. (2006) *Appl. Phys. Lett.*, **88**, 123502.
5 Sirringhaus, H., Kawase, T., and Friend, R.h. (2001) *MRS Bull.*, **26**, 539–543.
6 Gelinck, G.H., Huitema, H.E.A., van Veenendaal, E., Cantatore, E., Schrijnemakers, L., van der Putten, J.B.P.H., Geuns, T.C.T., Beenhakkers, M., Giesbers, J.B., Huisman, B.-H., Meijer, E.J., Benito, E.M., Touwslager, F.J., Marsman, A.W., van Rens, B.J.E., and de Leeuw, D.M. (2004) *Nat. Mater.*, **3**, 106–110.
7 Bronstein, H., Chen, Z., Ashraf, R.S., Zhang, W., Du, J., Durrant, J.R., Shakya Tuladhar, P., Song, K., Watkins, S.E., Geerts, Y., Wienk, M.M., Janssen, R.A.J., Anthopoulos, T., Sirringhaus, H., Heeney, M., and McCulloch, I. (2011) *J. Am. Chem. Soc.*, **133**, 3272–3275.
8 Yan, H., Chen, Z., Zheng, Y., Newman, C., Quinn, J.R., Dotz, F., Kastler, M., and Facchetti, A. (2009) *Nature*, **457**, 679–686.
9 Marks, T.J. (2010) *MRS Bull.*, **35**, 1018–1027.
10 Sze, S.M. and Ng, K.K. (2007) *Physics of Semiconductor Devices*, John Wiley & Sons, Inc.
11 Chen, Z., Lee, M.J., Shahid Ashraf, R., Gu, Y., Albert-Seifried, S., Meedom Nielsen, M., Schroeder, B., Anthopoulos, T.D., Heeney, M., McCulloch, I., and Sirringhaus, H. (2012) *Adv. Mater.*, **24**, 647.
12 Kim, F.S., Ahmed, E., Subramaniyan, S., and Jenekhe, S.A. (2010) *ACS Appl. Mater. Interfaces*, **2**, 2974–2977.
13 Meijer, E.J., de Leeuw, D.M., Setayesh, S., van Veenendaal, E., Huisman, B.-H., Blom, P.W.M., Hummelen, J.C., Scherf, U., and Klapwijk, T.M. (2003) *Nat. Mater.*, **2**, 678–682.
14 Babel, A., Zhu, Y., Cheng, K.-F., Chen, W.-C., and Jenekhe, S.A. (2007) *Adv. Funct. Mater.*, **17**, 2542–2549.
15 Szendrei, K., Jarzab, D., Chen, Z., Facchetti, A., and Loi, M.A. (2009) *J. Mater. Chem.*, **20**, 1317–1321.
16 Zaumseil, J. and Sirringhaus, H. (2007) *Chem. Rev.*, **107**, 1296–1323.
17 Ortiz, R.P., Facchetti, A., and Marks, T.J. (2009) *Chem. Rev.*, **110**, 205–239.
18 Bisri, S.Z. (2011) *Light-emitting transistors towards current-induced amplified spontaneous emission in organic single crystals*. Doctoral dissertation. Tohoku University, Sendai, Japan
19 Smits, E.C.P., Anthopoulos, T.D., Setayesh, S., van Veenendaal, E., Coehoorn, R., Blom, P.W.M., de Boer, B., and de Leeuw, D.M. (2006) *Phys. Rev. B*, **73**, 205316.
20 Bisri, S.Z. (2008) *Optoelectronic studies of organic single crystal transistors*. Master thesis. Tohoku University, Sendai, Japan
21 Loi, M.A., Rost-Bietsch, C., Murgia, M., Karg, S., Riess, W., and Muccini, M. (2006) *Adv. Funct. Mater.*, **16**, 41–47.
22 Street, R.A. and Salleo, A. (2002) *Appl. Phys. Lett.*, **81**, 2887.
23 Ishii, H., Sugiyama, K., Ito, E., and Seki, K. (1999) *Adv. Mater.*, **11**, 605–625.
24 de Boer, B., Hadipour, A., Mandoc, M.M., van Woudenbergh, T., and Blom, P.W.M. (2005) *Adv. Mater.*, **17**, 621–625.
25 Lei, C.H., Das, A., Elliott, M., Macdonald, J.E., and Turner, M.L. (2004) *Synth. Met.*, **145**, 217–220.
26 Anthopoulos, T.D., de Leeuw, D.M., Cantatore, E., van 't Hof, P., Alma, J., and Hummelen, J.C. (2005) *J. Appl. Phys.*, **98**, 054503.
27 Shkunov, M., Simms, R., Heeney, M., Tierney, S., and McCulloch, I. (2005) *Adv. Mater.*, **17**, 2608–2612.
28 Anthopoulos, T.D., Setayesh, S., Smits, E., Cölle, M., Cantatore, E., de Boer, B., Blom, P.W.M., and de Leeuw, D.M. (2006) *Adv. Mater.*, **18**, 1900–1904.
29 Walters, R.J., Bourianoff, G.I., and Atwater, H.A. (2005) *Nat. Mater.*, **4**, 143–146.
30 Misewich, J.A., Martel, R., Avouris, P., Tsang, J.C., Heinze, S., and Tersoff, J. (2003) *Science*, **300**, 783–786.

**31** Burroughes, J.H., Bradley, D.D.C., Brown, A.R., Marks, R.N., Mackay, K., Friend, R.H., Burns, P.L., and Holmes, A.B. (1990) *Nature*, **347**, 539–541.

**32** Friend, R.H., Gymer, R.W., Holmes, A.B., Burroughes, J.H., Marks, R.N., Taliani, C., Bradley, D.D.C., Santos, D.A.D., Bredas, J.L., Logdlund, M., and Salaneck, W.R. (1999) *Nature*, **397**, 121–128.

**33** Zaumseil, J., Donley, C.L., Kim, J.-S., Friend, R.H., and Sirringhaus, H. (2006) *Adv. Mater.*, **18**, 2708–2712.

**34** Chua, L.-L., Zaumseil, J., Chang, J.-F., Ou, E.C.-W., Ho, P.K.-H., Sirringhaus, H., and Friend, R.H. (2005) *Nature*, **434**, 194–199.

**35** Chen, Z., Lemke, H., Albert-Seifried, S., Caironi, M., Nielsen, M.M., Heeney, M., Zhang, W., McCulloch, I., and Sirringhaus, H. (2010) *Adv. Mater.*, **22**, 2371–2375.

**36** Kim, F.S., Guo, X., Watson, M.D., and Jenekhe, S.A. (2010) *Adv. Mater.*, **22**, 478–482.

**37** Cho, S., Lee, J., Tong, M., Seo, J.H., and Yang, C. (2011) *Adv. Funct. Mater.*, **21**, 1910–1916.

**38** Bürgi, L., Turbiez, M., Pfeiffer, R., Bienewald, F., Kirner, H., and Winnewisser, C. (2008) *Adv. Mater.*, **20**, 2217–2224.

**39** Dodabalapur, A., Katz, H.E., Torsi, L., and Haddon, R.C. (1996) *Appl. Phys. Lett.*, **68**, 1108.

**40** Sakamoto, Y., Suzuki, T., Kobayashi, M., Gao, Y., Fukai, Y., Inoue, Y., Sato, F., and Tokito, S. (2004) *J. Am. Chem. Soc.*, **126**, 8138–8140.

**41** Rost, C., Karg, S., Riess, W., Loi, M.A., Murgia, M., and Muccini, M. (2004) *Appl. Phys. Lett.*, **85**, 1613.

**42** Shi, J.W., Wang, H.B., Song, D., Tian, H.K., Geng, Y.H., and Yan, D.H. (2007) *Adv. Funct. Mater.*, **17**, 397–400.

**43** Wang, H., Wang, J., Yan, X., Shi, J., Tian, H., Geng, Y., and Yan, D. (2006) *Appl. Phys. Lett.*, **88**, 133508.

**44** Dinelli, F., Capelli, R., Loi, M.A., Murgia, M., Muccini, M., Facchetti, A., and Marks, T.J. (2006) *Adv. Mater.*, **18**, 1416–1420.

**45** Liu, C. and Sirringhaus, H. (2010) *J. Appl. Phys.*, **107**, 014516.

**46** Liu, C. and Sirringhaus, H. (2010) *Org. Electron.*, **11**, 558–563.

**47** Cho, S., Yuen, J., Kim, J.Y., Lee, K., Heeger, A.J., and Lee, S. (2008) *Appl. Phys. Lett.*, **92**, 063505.

**48** Wei, Q., Tajima, K., and Hashimoto, K. (2009) *ACS Appl. Mater. Interfaces*, **1**, 1865–1868.

**49** Rost, C., Karg, S., Riess, W., Loi, M.A., Murgia, M., and Muccini, M. (2004) *Appl. Phys. Lett.*, **85**, 1613.

**50** Unni, K.N.N., Pandey, A.K., Alem, S., and Nunzi, J.-M. (2006) *Chem. Phys. Lett.*, **421**, 554–557.

**51** Inoue, Y., Sakamoto, Y., Suzuki, T., Kobayashi, M., Gao, Y., and Tokito, S. (2005) *Jpn. J. Appl. Phys.*, **44**, 3663–3668.

**52** Arias, A.C., Corcoran, N., Banach, M., Friend, R.H., MacKenzie, J.D., and Huck, W.T.S. (2002) *Appl. Phys. Lett.*, **80**, 1695.

**53** Tada, K., Harada, H., and Yoshino, K. (1997) *Jpn. J. Appl. Phys.*, **36**, L718–L720.

**54** Tada, K., Harada, H., and Yoshino, K. (1996) *Jpn. J. Appl. Phys.*, **35**, L944–L946.

**55** Anthopoulos, T.D., Tanase, C., Setayesh, S., Meijer, E.J., Hummelen, J.C., Blom, P.W.M., and de Leeuw, D.M. (2004) *Adv. Mater.*, **16**, 2174–2179.

**56** Hayashi, Y., Kanamori, H., Yamada, I., Takasu, A., Takagi, S., and Kaneko, K. (2005) *Appl. Phys. Lett.*, **86**, 052104.

**57** Naber, R.C.G., Tanase, C., Blom, P.W.M., Gelinck, G.H., Marsman, A.W., Touwslager, F.J., Setayesh, S., and de Leeuw, D.M. (2005) *Nat. Mater.*, **4**, 243–248.

**58** Babel, A., Wind, J.D., and Jenekhe, S.A. (2004) *Adv. Funct. Mater.*, **14**, 891–898.

**59** Cho, S., Yuen, J., Kim, J.Y., Lee, K., and Heeger, A.J. (2006) *Appl. Phys. Lett.*, **89**, 153505.

**60** Aleshin, A.N., Shcherbakov, I.P., Petrov, V.N., and Titkov, A.N. (2011) *Org. Electron.*, **12**, 1285–1292.

**61** Pal, B.N., Trottman, P., Sun, J., and Katz, H.E. (2008) *Adv. Funct. Mater.*, **18**, 1832–1839.

**62** Babel, A. and Jenekhe, S.A. (2003) *Macromolecules*, **36**, 7759–7764.